Pathophysiological Changes in Rhesus Monkeys with Paraquat-Induced Pulmonary Fibrosis

Mingyang Shao[1] · Sha Yang[2] · Aiyi Zheng[2] · Zhenru Wu[1] · Menglin Chen[1] · Rong Yao[2] · Yujun Shi[1] · Gen Chen[3]

Abstract

Purpose Pulmonary fibrosis is a life-threatening lung disorder. A comprehensive understanding of the pathophysiological changes in the development of pulmonary fibrosis will lead to new insights into its treatment.

Methods We used a paraquat (PQ)-induced rhesus monkey model of pulmonary fibrosis to comprehensively investigate the process of pulmonary fibrosis development. Rhesus monkeys were orally administered PQ at concentrations of 25 mg/kg, 40 mg/kg, and 80 mg/kg. The dose was given once. Behavior and clinical data, such as PQ concentration, arterial oxygen saturation, biochemical evaluation, lung histopathology, and medical imaging, were continuously observed.

Results Paraquat-exposed monkeys developed pulmonary fibrosis following an expected time course, especially at 25 mg/kg. CT images showed ground-glass lesions in the lung after 4 weeks, and pulmonary fibrosis persisted until the end of follow-up. Using pathological examination, the lung sustained collagen deposition and slight inflammatory cell infiltration. All rhesus monkeys had obvious inflammatory infiltration within 1 week according to the immunohistochemical results and the number of leukocytes in the blood. The CT results showed that pulmonary fibrosis had not formed, indicating that drugs with powerful anti-inflammatory ability are potential candidates for early pulmonary fibrosis treatment.

Conclusion Our study describes the dynamic process of paraquat-induced pulmonary fibrosis in rhesus monkeys and provided a pathophysiological basis for the treatment of pulmonary fibrosis.

Keywords Pulmonary fibrosis · Paraquat · Rhesus monkey · CT scan · CT-guided percutaneous lung biopsy

Introduction

Pulmonary fibrosis is a life-threatening disease characterized by progressive dyspnea and worsening of pulmonary function [1]. It manifests as progressive pulmonary interstitial fibrous tissue hyperplasia, significant thickening of alveolar walls, and reduction of pulmonary capillaries, leading

✉ Rong Yao
  yaorong@wchscu.cn

1 Institute of Clinical Pathology, Key Laboratory of Transplant Engineering and Immunology, West China Hospital, Sichuan University, 37 Guoxue Alley, Wuhou, Chengdu 610041, China

2 The Emergency Department, West China Hospital, Sichuan University, 37 Guoxue Alley, Wuhou, Chengdu 610041, China

3 Development and Application of Human Major Disease Monkey Model Key Laboratory of Sichuan, Sichuan Yibin Horizontal and Vertical Biotechnology Co., Ltd., Yibin 644601, China

to pulmonary vein and pulmonary hypertension and severe right heart failure [2]. Treatment of pulmonary fibrosis with pirfenidone and nintedanib has been shown to slow disease progression, but these drugs do not cure pulmonary fibrosis [3]. In particular, patients with severe COVID-19 develop pulmonary fibrosis [4]. To understand the pathogenesis and clinical treatment of pulmonary fibrosis, it is important to use large nonhuman primate models to examine the process of pulmonary fibrosis panoramically and dynamically.

To understand the process of pulmonary fibrosis in animals, a simple, convenient, and efficient animal model for pulmonary fibrosis is needed. At present, methods of inducing pulmonary fibrosis in animals are mainly divided into two categories: biological factors and nonbiological factors. Models induced by biological factors are more common in the study of cytokine overexpression or when targeting type II alveolar epithelial cell injury [5, 6]. These models are more similar to the late clinical manifestations of pulmonary fibrosis, but are also more expensive. Induction by abiotic factors has the advantages of diversity in

drug selection and administration routes, simple operation and low price, and is therefore a more common choice for modeling pulmonary fibrosis. This modeling approach is mainly based on drug or toxic factors (e.g., bleomycin or paraquat), environmental factors (e.g., silica or asbestos), and other factors [7]. At present, the most common method is animal pulmonary fibrosis induced by bleomycin. However, this modeling method has many shortcomings, such as high animal mortality, complicated operation, severe acute lung injury, mild collagen metabolism disorder, and uneven distribution of lesions [8–10]. In models induced by environmental factors, the best inducer is silicon dioxide [11]. However, it is rarely used because the environmental factors pose risk to the human body during the modeling process. Therefore, a more convenient and consistent model of the pathogenesis of pulmonary fibrosis is still needed.

In recent years, many researchers have used paraquat to induce pulmonary fibrosis in animals. Paraquat (PQ) is a fast-acting and nonselective contact herbicide. The lungs are a specific target for the pathological effects of PQ because of its selective accumulation by this organ. PQ pulmonary concentrations can be 6 to 10 times higher than those in the plasma [12]. Many patients with PQ poisoning may develop lung damage and subsequently develop pulmonary fibrosis after ingestion of PQ of at least 20 mg/kg by oral, inhalation, and skin exposure. If PQ intake is higher than 40 mg/kg, it will cause shock and lethality within 24–48 h [13]. In addition, PQ can also successfully induce pulmonary fibrosis in experimental animals such as mice, rats, and rabbits, usually by a one-time oral perfusion or intraperitoneal injection [14–16]. The method of PQ-induced pulmonary fibrosis avoids non-specific damage and can be specifically enriched in the lungs to form lung damage. Therefore, the PQ-induced animal model may be a simple, rapid, and consistent method of modeling pulmonary fibrosis.

Due to the lack of knowledge of the pathophysiological process in the pathogenesis of pulmonary fibrosis, the development of therapeutic strategies has been largely hindered. The current knowledge of the pathophysiological processes underlying pulmonary fibrosis comes from small animal studies and is limited by substantial differences in species. Most laboratory animals, such as rodents, require specialized imaging facilities, and the ability to assess lung injury with imaging is limited by other factors as well. It is also difficult to obtain enough arterial blood from rodents, especially mice, thus making it infeasible to generate continuous dynamic data from an individual animal [17]. To avoid these problems, we chose rhesus monkeys as model animals in our study. They are phylogenetically similar to humans, so they have similarities in related behaviors, anatomy, and physiology, and the degree of pulmonary fibrosis can be assessed by computed tomography (CT), which can provide a more comprehensive understanding of the dynamic process of pulmonary fibrosis.

At present, there are almost no reports on PQ-induced pulmonary fibrosis in rhesus monkey models. Hui Chen et al. reported 80 mg/kg PQ-induced pulmonary fibrosis using intragastric intoxication in Wistar rats [18]. Experimental dosages were calculated according to the surface area-to-volume ratio and were equivalent to 55 mg/kg (in rhesus monkey terms). However, the method and dosage of PQ-induced pulmonary fibrosis in mice and Wistar rats are not identical [18–22]. To fully understand the development process of pulmonary fibrosis in nonprimate animals, we used orally-administered paraquat in rhesus monkeys to construct a pulmonary fibrosis model. We recorded the continuous clinical data of rhesus monkeys induced by oral doses of PQ at 25 mg/kg, 40 mg/kg, and 80 mg/kg. Among these, oral paraquat at 25 mg/kg was the most effective in inducing pulmonary fibrosis, which we discuss in detail, including biochemical indicators, CT, and pathological results. Inflammation is more pronounced in the first week and can be treated with anti-inflammatory agents. In the later stage, fibrosis occurs without obvious inflammation, and treatment for pulmonary fibrosis is needed. Our data can provide an experimental basis for exploring the pathophysiology of pulmonary fibrosis and evaluating potential treatment strategies.

Materials and Methods

Animals

The animal protocols used in this study were approved by the Animal Ethics Committee of West China Hospital of Sichuan University (approval number, 2020093A). Healthy adult experimental rhesus monkeys were provided by Chengdu Ping'an Experimental Animal Reproduction Center (License No.: SCXK [CHUAN] 2014–013, Chengdu, China). The monkeys were housed singly in standard cages with a 12-h light/dark cycle. For all invasive operations, the monkeys were anesthetized using ketamine and propofol for subsequent intubation and ventilation using isoflurane to maintain anesthesia. All monkeys were provided with standard dry monkey food and water ad libitum. The monkeys were scheduled for euthanasia when they displayed the following symptoms: inability to eat and drink, flapping tremor, and inability to wake up. Rhesus monkeys were submitted to a full necropsy after death.

Experimental Design and Treatments

All rhesus monkeys in this experiment were male, weighing between 4 and 5 kg, and were born in 2014. Based on previous data [13, 18], we used different doses in the process of

constructing PQ-induced models of pulmonary fibrosis in rhesus monkeys, including 25 mg/kg, 40 mg/kg, and 80 mg/kg of PQ administered orally. The experiments were conducted simultaneously. Since rhesus monkeys are expensive and not readily available, we performed experiments with only three rhesus monkeys per group.

In this experiment, rhesus monkeys were fasted for a day before induction. The anesthetized rhesus monkeys were given PQ orally once by gavage. They then underwent CT scanning on a regular basis at the West China Hospital of Sichuan University. The arterial blood of rhesus monkeys was extracted to measure arterial oxygen saturation and serum potassium, as well as other indicators. Venous blood was collected, and lung puncture was performed. Autopsy performed after rhesus monkey dies.

CT-guided Lung Biopsy

All procedures were performed by interventional radiologists experienced in performing percutaneous lung biopsies. During the time of biopsy, CT images through the area of interest were obtained in helical scan mode using a 3- to 5-mm thickness to avoid emphysematous lung and pulmonary vessels and cross the smallest number of pleural surfaces. Rhesus monkeys were in a supine position to provide the shortest and safest route for lung biopsy. The rhesus monkey's chest required skin preparation and was prepped with an antiseptic solution and then local anesthesia using 1% lidocaine. A 19-gauge puncture needle was introduced, and new tomographic images were obtained to confirm and modify the needle position. After the procedure, a chest CT scan was routinely performed to detect the presence of possible complications. The biopsy tract in the lung was gently injected with 3 to 5 mL of sterile 0.9% saline while withdrawing the coaxial sheath.

Transbronchial Lung Biopsy (TBLB)

After determining the most suitable PQ-induced rhesus monkey pulmonary fibrosis model, we selected three rhesus monkeys to explore the dynamic physiological process of early pulmonary fibrosis. We collected bronchoalveolar lavage fluid (BALF) from rhesus monkeys at 25 mg/kg at 12, 36, and 60 h.

A fiberoptic bronchoscope was used to reach the selected segmental bronchus. The biopsy forceps were advanced, and then withdrawn 1–2 cm until resistance was encountered. Generally, it entered a depth of 4 cm from the segmental bronchus opening. The biopsy forceps were then opened, and the forceps were advanced by an additional 1 cm at the end of expiration. Then, the tissue was clamped and quickly withdrawn.

Histology

We performed immunohistochemistry on the monkey lung and other organ specimens. For hematoxylin and eosin (HE) staining and Masson and Sirius red staining, tissues were fixed in 10% neutral buffered formalin for 48 h, embedded in paraffin, sectioned at 5 μm, and stained. Immunohistochemistry for CD68 (1:100, Abcam, Cambridge, UK) and F4/80 (1:100, Abcam, Cambridge, UK) was used to label pulmonary macrophages. MAC387 (1:200, Thermo Fisher, Grand Island, NY) is a monocyte marker that is positively expressed during early infiltration in certain inflammatory states. We used α-SMA (1:200, Abcam, Cambridge, UK) as an immunohistochemical marker of alpha-smooth muscle actin, a feature of myofibroblasts. Lung pathology analyses were performed by two pathologists independently.

Behavioral Testing

During this study, the behaviors of the rhesus monkeys were observed every day, including self-biting, self-grabbing, eye-poke, finger sucking, hair pulling, bouncing, shaking, body turning and stepping, eating, yawning, cage shaking, exploring, and foraging.

Biochemical Analyses

Blood serum, plasma, and BALF were isolated by centrifugation at $1500 \times g$ for 10 min at 4 °C for biochemical evaluation and PQ concentration detection. All the parameters were analyzed in a standard clinical laboratory at West China Hospital, Sichuan University.

Results

We first analyzed the performance of the rhesus monkeys after PQ poisoning. Rhesus monkeys behaved normally in the initial stage, but within 12–30 h, they exhibited one or more of the following clinical symptoms: lethargy, decreased activity, vomiting, abdominal distension, and drooling. Rhesus monkeys treated with 25 mg/kg and 40 mg/kg PQ survived until the end of follow-up, while rhesus monkeys treated with 80 mg/kg PQ died after 1 week (Supplementary Fig. 1).

The concentration of PQ in rhesus monkey blood was the highest at 12 h. At that point, the PQ concentration in the blood of those treated with 25 mg/kg was 170.83 ng/mL (Fig. 1A). The PQ concentration in the blood of those treated with 40 mg/kg was 330.33 ng/mL. The PQ concentration in the blood of those treated with 80 mg/kg was 966.75 ng/mL
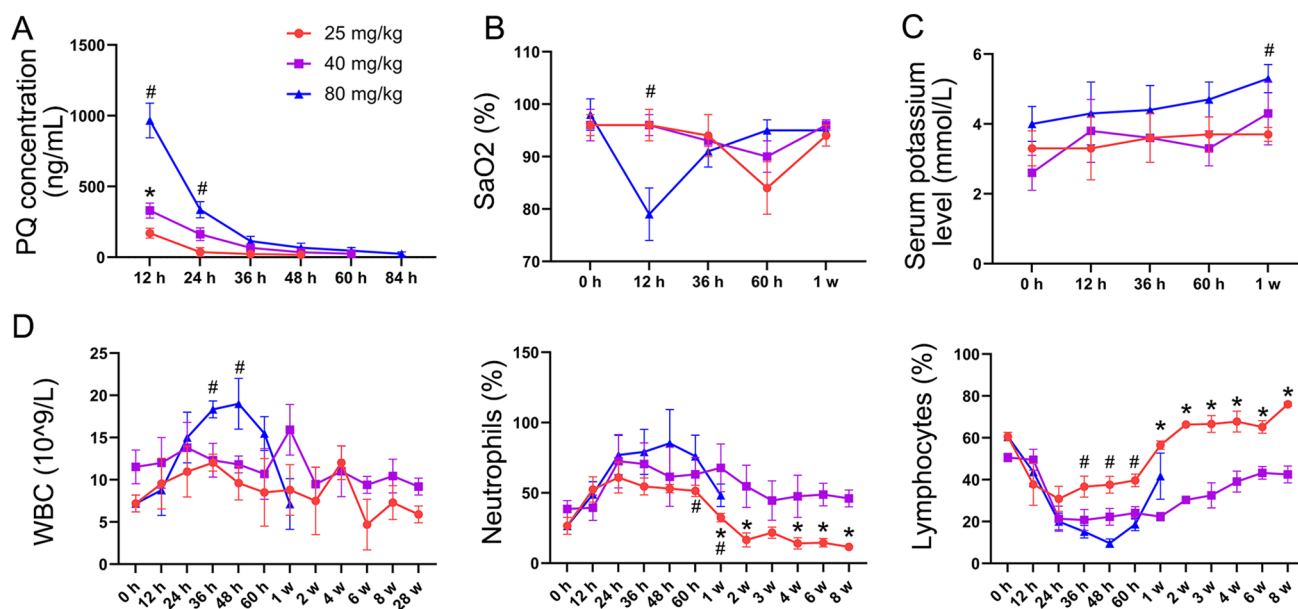
Fig. 1 Blood results in a rhesus monkey model with pulmonary fibrosis induced by oral PQ at 25, 40, or 80 mg/kg. **B** Changes in arterial oxygen saturation (SaO₂) during modeling. **C** Changes in serum potassium concentration. **D** Counts of white blood cells, neutrophils, and lymphocytes in blood. The B–D legend is the same as A.

PQ paraquat. Data are presented as the mean ± SEM (error bars). $n = 3$ per group. Between-group comparison at 25 mg/kg vs. 40 mg/kg, $*p < 0.05$. Between-group comparison at 25 mg/kg vs. 80 mg/kg, $\#p < 0.05$

at 12 h and 114.56 ng/mL at 36 h (Fig. 1A, Supplementary Fig. 2A). Over time, the concentration of PQ in the blood decreased until it was undetectable.

The blood pressure of the rhesus monkeys did not change significantly. The arterial oxygen saturation (SaO2) of the rhesus monkeys treated with 25 or 40 mg/kg PQ decreased briefly at 60 h. However, the SaO2 of the rhesus monkeys treated with 80 mg/kg decreased at 12 h (Fig. 1B, Supplementary Fig. 2B). Hypokalemia is a negative prognostic marker in paraquat poisoning [23]. Therefore, we analyzed the serum potassium concentration. There was a slight fluctuation in serum potassium concentration in rhesus monkeys treated with 25 or 40 mg/kg PQ. The serum potassium of rhesus monkeys treated with 80 mg/kg PQ increased to 5.3 mmol/L at 1 week (Fig. 1C, Supplementary Fig. 2C). The proportion of white blood cells and neutrophils in their blood increased in the early stage of PQ poisoning and returned to normal 1 week later (Fig. 1D, Supplementary Fig. 2D).

Serum levels of alanine transaminase (ALT) and aspartate transaminase (AST) in the blood of rhesus monkeys treated with 25 or 40 mg/kg PQ increased from 12 to 60 h and then gradually decreased. In rhesus monkeys treated with 80 mg/kg PQ, AST increased significantly at 12 to 48 h, but ALT did not change significantly (Fig. 2A, Supplementary Fig. 3A). Markers of renal function, such as creatinine (CREA), uric acid (UA), and urea, of rhesus monkeys treated with 40 mg/kg PQ was higher than normal in the first

4 weeks. Rhesus monkeys treated with 25 or 80 mg/kg PQ showed only small fluctuations in renal function (Fig. 2B, Supplementary Fig. 3B). Creatine kinase (CK), hydroxybutyrate dehydrogenase (HBDH) and lactate dehydrogenase (LDH) are relevant markers for cardiac injury, hepatic or muscle injury, and hemolysis. These markers were significantly increased in the early stage and essentially returned to normal 2 weeks later (Fig. 2C, Supplementary Fig. 3C).

The CT images of rhesus monkeys induced with 25 mg/kg PQ were evaluated as follows. At 12 h, pneumomediastinum appeared in the lungs, with exudative changes in both lungs. At 60 h, the right lung was atelectatic, and there was a small amount of exudate in the middle lobe. After 1 week, the lung markings were disorganized, with left subpleural changes and thickening of the interlobar fissures (Fig. 3A). At 4 weeks, ground-glass lesions appeared in the lungs. Diffuse ground-glass lesions were more obvious at 12 weeks. The CT results revealed that pulmonary fibrosis may have developed in rhesus monkeys after 4 weeks (Fig. 3B, Supplementary Table 1).

Lung CT images of rhesus monkeys treated with 40 mg/kg PQ showed obvious mediastinal emphysema at 12 h. At 60 h, there was pneumothorax and hemorrhage in the right lung. The apex of the upper lobe of the lung showed consolidation exudation, compressed atelectasis, pleural effusion, and mediastinal emphysema aggravation. Mediastinal emphysema disappeared at 1 week (Fig. 3A). At 4 weeks, pneumothorax and mediastinal emphysema appeared again
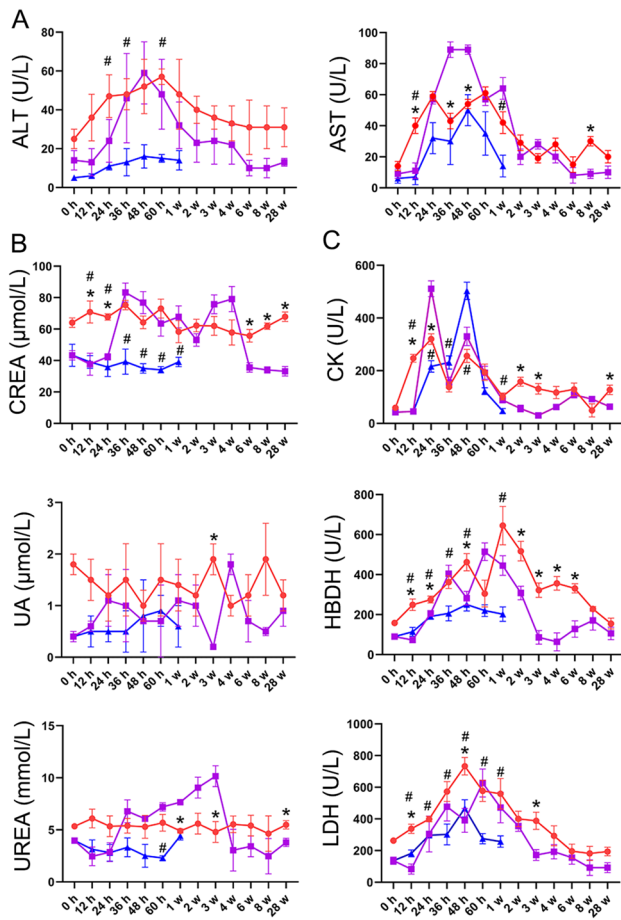
Fig. 2 The results of liver function, kidney function, and cardiac enzyme profile in the blood of three rhesus monkeys. **A** Changes in ALT and AST. **B** The contents of CREA, UA, and UREA in renal function in serum with the passage of time. **C** Change trend of related indices of cardiac enzyme profile. The B–D legend is the same as in A. *AST* aspartate aminotransferase, *ALT* alanine aminotransferase, *CREA* creatinine, *UA* uric acid, *CK* creatine kinase, *HBDH* hydroxybutyrate dehydrogenase, *LDH* lactate dehydrogenase. Data are presented as the mean $\pm$ SEM (error bars). $n = 3$ per group. Between-group comparison at 25 mg/kg vs. 40 mg/kg, $*p < 0.05$. Between-group comparison at 25 mg/kg vs. 80 mg/kg, $^\#p < 0.05$

in the lungs, and there was a small bilateral subpleural effusion. Atelectasis was also observed at 5 weeks, and there was no pulmonary fibrosis detected by CT until 8 weeks (Fig. 3C, Supplementary Table 1). Rhesus monkeys treated with 40 mg/kg PQ showed a more severe progression compared to the clinical pulmonary fibrosis course, but no obvious fibrosis was seen by CT until 8 weeks. In addition, CT images of rhesus monkeys treated with 80 mg/kg PQ also did not show pulmonary fibrosis.

We further observed the pathological changes in the lung during the induction of pulmonary fibrosis by histopathology of lung biopsy samples. Lung biopsy tissue samples of rhesus monkeys treated with 25 mg/kg PQ showed extensive cellular thickening of the interalveolar septa, inflammatory cell infiltration, and alveolar structural disorder or destruction in the early stages. The results of Masson's trichrome staining and Sirius red staining also indicated that PQ may have induced excessive collagen deposition in lung tissue (Fig. 4, Supplementary Fig. 4, Supplementary Table 2). After 1 week, it still displayed inflammatory cell infiltration, increased interstitial cells with a fibroblastic appearance, and fibrogenesis. After 4 weeks, lung tissue exhibited fibrosis and obvious inflammatory infiltration (Fig. 5, Supplementary Fig. 4). We used α-SMA as an immunohistochemical marker of alpha-smooth muscle actin, a feature of myofibroblasts. The results showed significant collagen deposition at 12 weeks (Fig. 5). The α-SMA staining was consistent with the results of Masson staining (Fig. 5). The expression of α-SMA was high at 4–12 weeks in the rhesus monkeys treated with 25 mg/kg. Even at 12 weeks, pulmonary fibrosis was still present, which was consistent with the CT results.

The lungs of the rhesus monkeys treated with 40 mg/kg PQ showed diffuse hemorrhage at an early stage. Collagen deposition appeared at all time points after 1 week (Fig. 4, Supplementary Table 2). From 1 to 2 weeks, inflammatory cells infiltrated and exuded obviously in the alveolar cavity (Fig. 5). Masson and Sirius red staining showed collagen deposition up to 8 weeks. The α-SMA staining results were consistent with the Masson and Sirius red staining results.

After 1 week, rhesus monkeys treated with 80 mg/kg PQ died of poisoning. Lung histopathology showed mild inflammation and no obvious collagen deposition. However, alveolar edema and collapse were observed. Hemorrhagic foci were observed in the lung tissue. High doses of oral PQ also caused intestinal mucosal cell shedding. The liver and kidneys were also damaged (Fig. 6).

We found that oral administration of 25 mg/kg PQ in rhesus monkeys was more consistent with the development of pulmonary fibrosis. To understand the early changes in the lung at this dose, we replicated PQ poisoning in rhesus monkeys with an oral dose of 25 mg/kg. Then, BALF and lung tissues from transbronchial lung biopsies were collected. The concentration of PQ in BALF was 46.7 ng/mL (Fig. 7A). In the BALF, white blood cells increased at 12 h and gradually returned to normal (Fig. 7B). The biochemical indices of the rhesus monkeys treated with 25 mg/kg peaked at 36 h and then returned to normal (Fig. 7C). Lung tissue sections obtained by transbronchial lung biopsy displayed extensive cellular thickening of the interalveolar septa, interstitial edema, and inflammatory cell infiltration. The results demonstrated that the alveolar structure was damaged, with extensive collagen deposition at 36 h and 60 h (Fig. 7D).
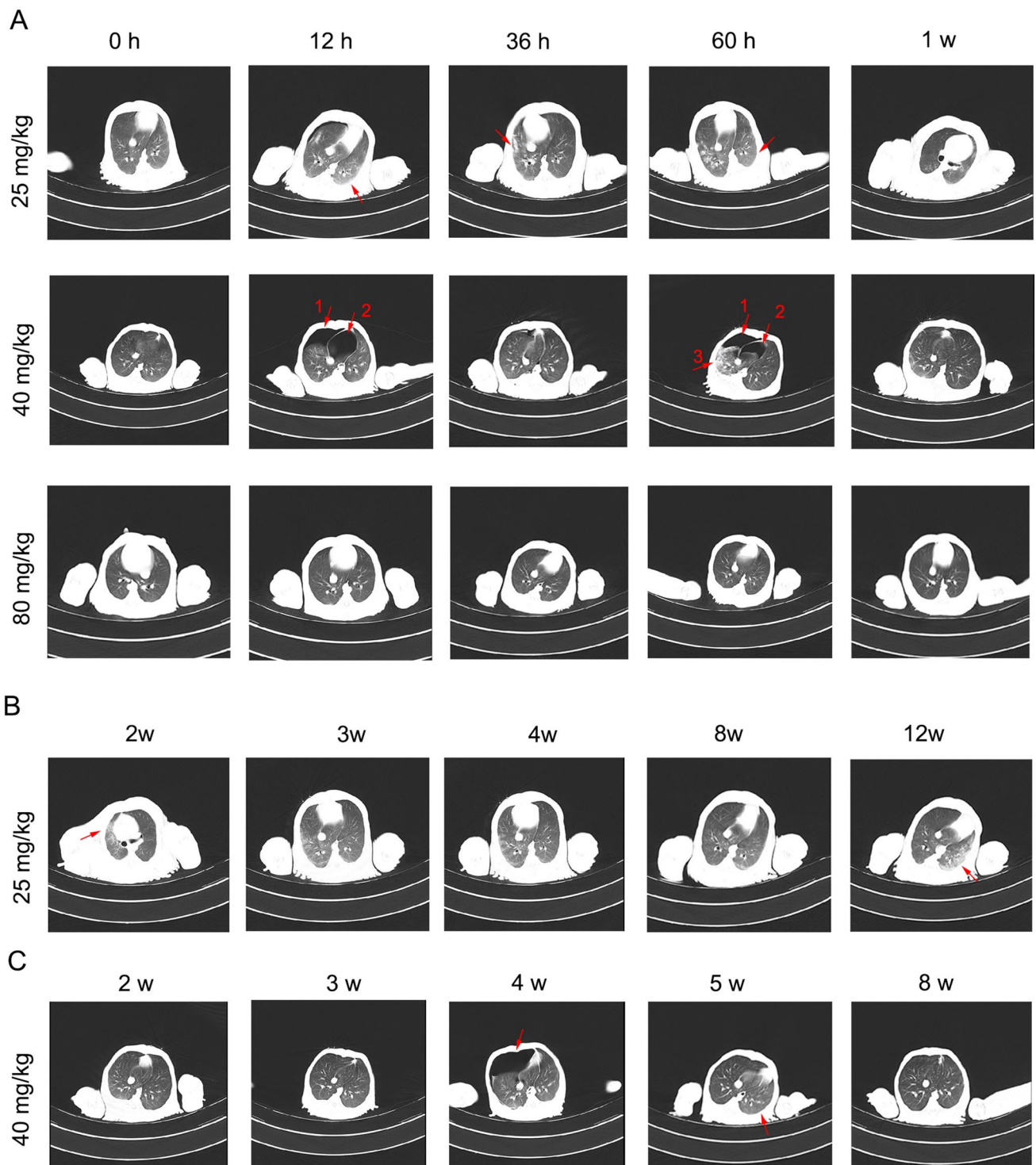
Fig. 3 Computed tomography (CT) imaging results of rhesus monkeys. **A** The results of rhesus monkeys during the early stages of PQ induction. **B** In rhesus monkeys treated with 25 mg/kg PQ, ground-glass lesions after 4 weeks of follow-up. **C** CT of rhesus monkeys treated with 40 mg/kg PQ during weeks 2–8. Arrows are annotated as follows: in the 25 mg/kg group, exudative changes in both lungs at 12 h; exudation in the upper left lung at 36 h; right atelectasis at 60 h; right lung shrinkage and poor light transmittance at 2 weeks; ground-glass lesions at 12 weeks. In the 40 mg/kg group, pneumothorax ①, mediastinal emphysema ② occurred at 12 h; pneumothorax ①, mediastinal emphysema ②, lung apex consolidation exudation ③ at 60 h; pneumothorax occurred at 4 weeks; atelectasis occurred at 5 weeks
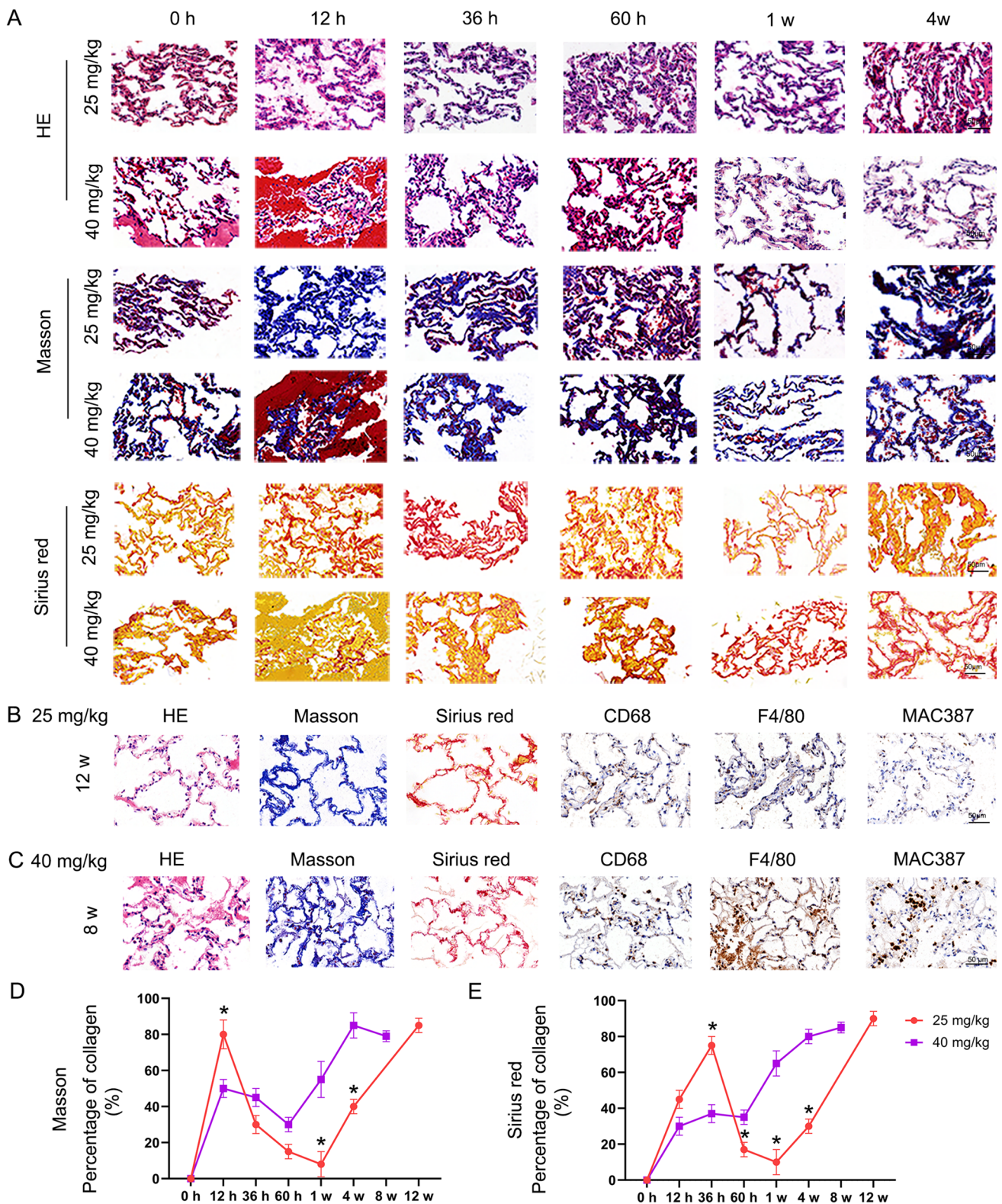
Fig. 4 Lung histopathological results of three PQ-poisoned rhesus monkeys. **A** The results of HE, Masson and Sirius red staining in lung tissue. **B** Pathological results of rhesus monkeys poisoned with 25 mg/kg PQ for 12 weeks. **C** The results of rhesus monkeys poi-soned with 40 mg/kg PQ for 8 weeks. **D** and **E** was the semi-quanti-tative statistical result of collagen on Masson staining and Sirius red staining, respectively. Scale bars = 50 μm
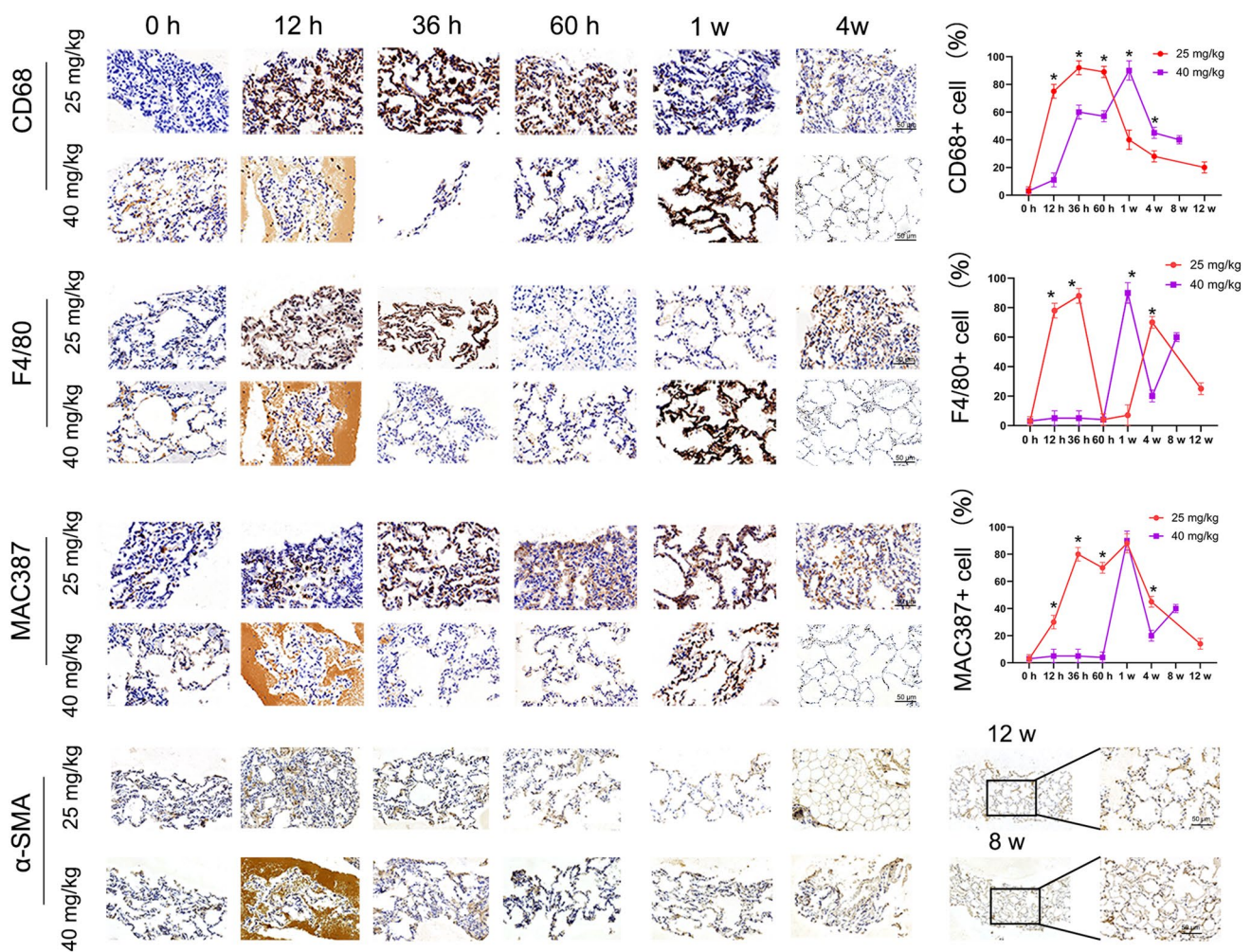
Fig. 5 The IHC results of CD68, F4/80, MAC 387, and α-SMA in lung tissue. Between-group comparison at 25 mg/kg vs. 40 mg/kg, *p < 0.05

Discussion

PQ poisoning involves acute damage to multiple organs, including the liver, heart, kidneys and lungs. There are two clinical stages in the development of lung lesions, which are divided into early-stage acute lung injury and late-stage pulmonary fibrosis [24]. In the first week of induction with PQ, we also found that rhesus monkeys developed more obvious acute lung injury (ALI). ALI can further lead to respiratory distress and eventually develop into pulmonary fibrosis [25, 26]. We observed early-stage ALI, including the tissue infiltration of inflammatory cells, pulmonary edema, and arterial hypoxemia, which damage the vascular endothelium and alveolar epithelium, thus diminishing lung function. Thus, drugs with powerful anti-inflammatory ability are potential candidates for early pulmonary fibrosis treatment.

During the experiment, we found inconsistencies between CT images and pathological results. Masson and Sirius red within 60 h after oral administration of 25 mg/kg PQ in rhesus monkeys showed a large amount of collagen exudation, while the CT showed no significant change. In addition, before the death of the rhesus monkey model orally administered 80 mg/kg PQ, there was no significant abnormality in medical imaging, but there was alveolar edema and collapse in lung pathology, and obvious bleeding on the lung surface could be observed in autopsy results. This difference is clinically important and should not be ignored. Kelahan LC et al. suggest that when an image-guided biopsy is finished, if the resulting pathologic diagnosis does not appear consistent (concordant) with the imaging findings that prompted the biopsy, this should prompt further evaluation [27]. Therefore, respiratory physicians and radiologists need to be informed that there is a discrepancy between CT images and pathology after drug poisoning, which can be used as a reference in clinical treatment.

The timeline of the laboratory values, histology and CT follow-up were different. We closely tracked the performance of rhesus monkeys treated with 25 or 40 mg/kg
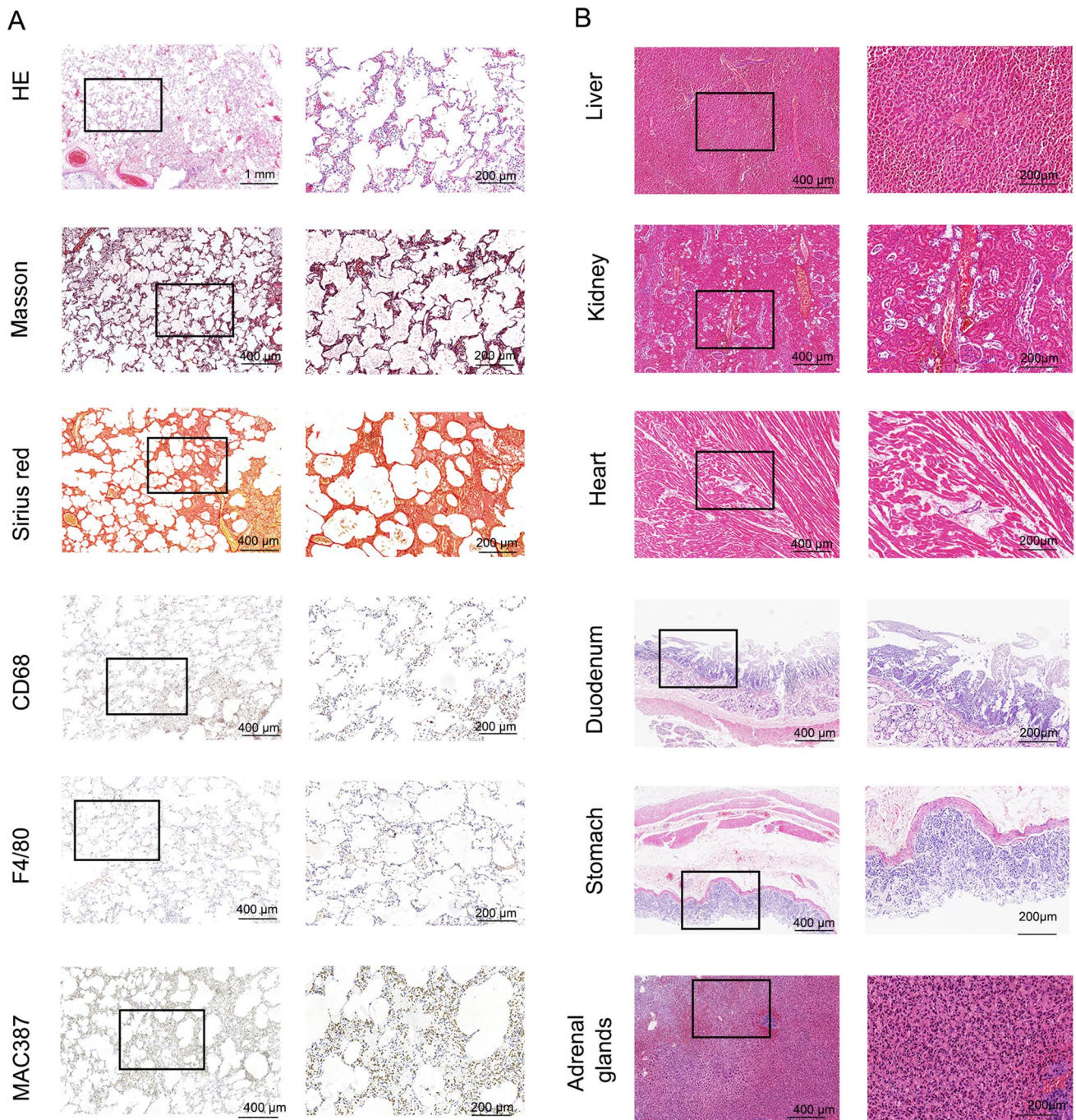
Fig. 6 Autopsy lung pathology results of 80 mg/kg PQ-poisoned rhesus monkeys at 1 week (**A**) and HE staining of other organs (**B**). Scale bars = 200 μm

PQ until 8 weeks and found that only 25 mg/kg PQ rhesus monkeys showed similar clinical pulmonary fibrosis from 4 weeks by CT and histopathology. To determine the stability of the 25 mg/kg PQ model, we continued to focus on 12 weeks to determine the stable presence of pulmonary fibrosis in this model. Due to the high cost of CT and biopsy and the need for experienced clinicians to operate, we only

collected laboratory values to determine the animal's survival status, routine blood test and degree of organ damage during follow-up after 12 weeks.

In our study, the results of Masson and Sirius red staining showed that both the 25 mg/kg and 40 mg/kg groups had collagen deposition after 4 weeks, but the CT results showed that only the 25 mg/kg group had obvious ground-glass
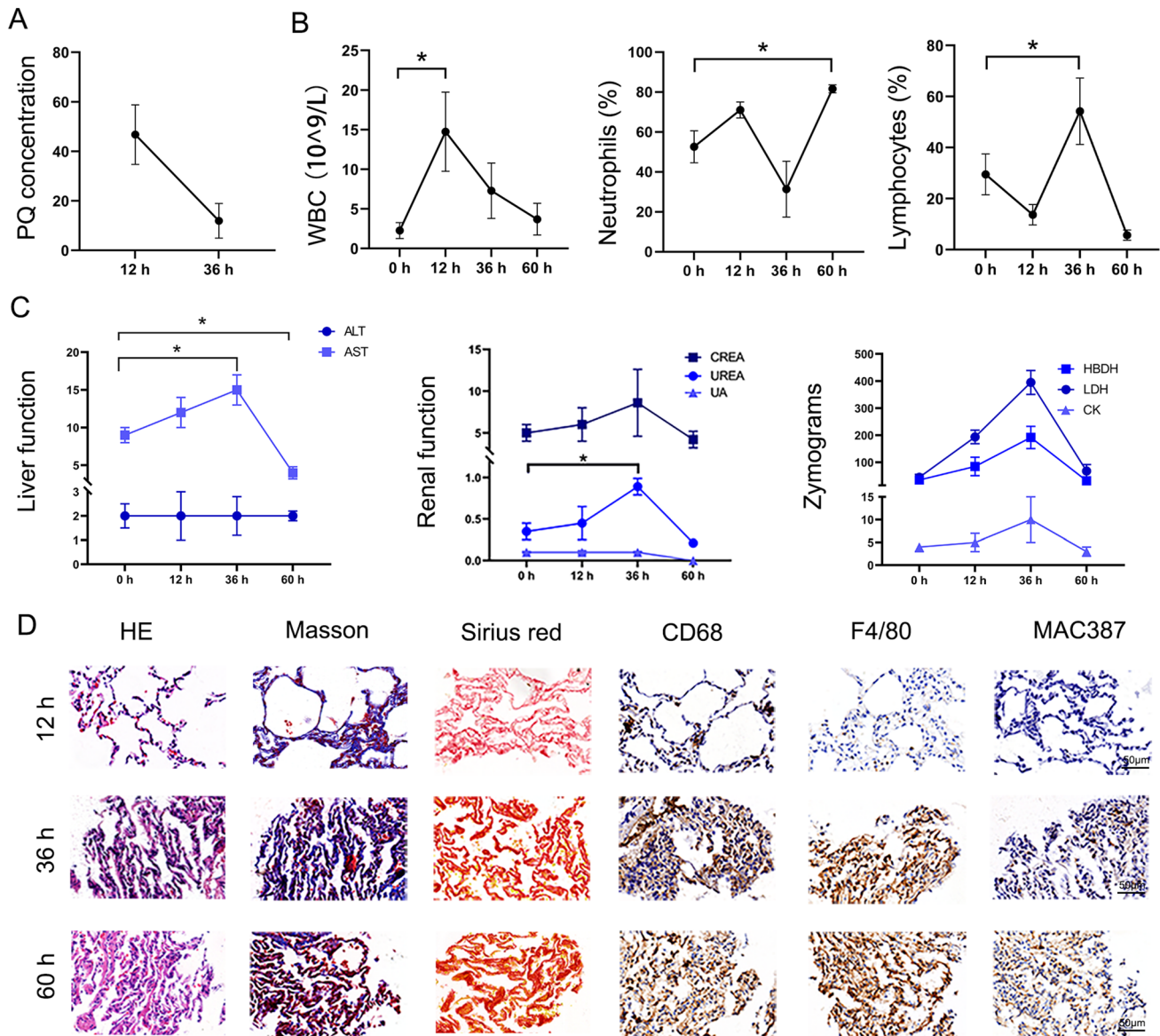
Fig. 7 BALF results and transbronchial lung biopsy histopathology of rhesus monkeys treated orally with 25 mg/kg PQ. **A** PQ concentration in BALF. **B** Classification of white blood cells, neutrophils, and lymphocytes in BALF. **C** Changes in liver function, kidney function, and myocardial enzyme profile in BALF. **D** Pathology results of transbronchial lung biopsy. *BALF* bronchoalveolar lavage fluid, *PQ* paraquat. Scale bars = 50 μm. $n = 3$ per group

lesions at a later stage, while not observed in the 40 mg/kg group. But we don't know the reason for this phenomenon. We hypothesize that this experiment had the disadvantage that the sample size was not large enough, which may mislead our conclusions. In addition, clinically, moderate to severe poisoning usually occurs after ingestion of 20–40 mg/kg. Patients may develop pulmonary fibrosis, but pulmonary fibrosis may not appear for days or weeks [28]. In terms of clinical outcomes, pulmonary fibrosis may not be entirely dose-dependent. The 40 mg/kg group had severe pulmonary exudation and edema (Fig. 4 at 12 h), and pneumothorax (Fig. 3 at 12 h, 60 h, and 4 w) also showed moderate to severe poisoning. Rhesus monkeys did not develop pulmonary fibrosis for several weeks, which was similar to the clinical phenomenon. We hope to expand the sample size to verify the experimental results in the future.

Although this study provides a dynamic model of the pathophysiological process of rhesus monkeys during pulmonary fibrosis, there are still many deficiencies. First, rhesus monkeys are too expensive to be validated as a model in large numbers, which is a shortcoming of this study. Second, the absorption of PQ occurs mainly in the small intestine [29]. In this experiment, rhesus monkeys were fasted for a day before modeling, but CT images showed that they still

had food residues in their stomachs. This may have impacted the results. Third, most of the lung tissues in this study were obtained by biopsy, and the samples were small, so the fibrosis of the whole lung could not be determined by pathology, which affected the convincingness of the conclusion. Fourth, although we provided CT scan information, there were no data on lung function in these animals, which was a limitation of the experimental conditions.

Because the pathogenesis of pulmonary fibrosis is not fully understood, no efficient therapeutics have been developed to treat this condition. The large species difference between small animals and humans, as well as the lack of information on the early changes in lung tissue and the internal environment, have hindered the understanding of the pathophysiological processes in pulmonary fibrosis. We followed the pathophysiology of toxin-induced pulmonary fibrosis in nonhuman primates, including changes in clinical features, histopathology, imaging, and lifespan. Clinical manifestations of pulmonary fibrosis in nonhuman primates may be used to investigate the mechanisms underlying the initiation and development of pulmonary fibrosis, providing a research basis for the follow-up exploration of pulmonary fibrosis treatment.

Conclusions

In summary, we used a large, nonhuman primate model to provide novel insights into the pathophysiological process of pulmonary fibrosis. Our work demonstrates that inflammatory infiltration is prominent in the early stage and may play an important role in the development of pulmonary fibrosis as a potential therapeutic target for this disease. In addition, the rhesus monkey model with oral administration of 25 mg/kg PQ is more similar to the natural process of pulmonary fibrosis, and therefore has the potential to be used for drug development for pulmonary fibrosis.

Declarations

References

1. Li A, Chen JY, Hsu CL, Oyang YJ, Huang HC, Juan HF (2022) A single-cell network-based drug repositioning strategy for post-COVID-19 pulmonary fibrosis. Pharmaceutics 14:971. https://doi.org/10.3390/pharmaceutics14050971

2. Galdino de Souza D, Santos DS, Simon KS, Morais JAV, Coelho LC, Pacheco TJA, Azevedo RB, Bocca AL, Melo-Silva CA, Longo JPF (2022) Fish oil nanoemulsion supplementation attenuates bleomycin-induced pulmonary fibrosis BALB/c mice. Nanomaterials (Basel) 12:1683. https://doi.org/10.3390/nano12101683

3. Mei Q, Liu Z, Zuo H, Yang Z, Qu J (2022) Idiopathic pulmonary fibrosis: an update on pathogenesis. Front Pharmacol 12:797292. https://doi.org/10.3389/fphar.2021.797292

4. George PM, Wells AU, Jenkins RG (2020) Pulmonary fibrosis and COVID-19: the potential role for antifibrotic therapy. Lancet Respir Med 8:807–815. https://doi.org/10.1016/S2213-2600(20)30225-3

5. Sun L, Louie MC, Vannella KM, Wilke CA, LeVine AM, Moore BB, Shanley TP (2011) New concepts of IL-10-induced lung fibrosis: fibrocyte recruitment and M2 activation in a CCL2/CCR2 axis. Am J Physiol Lung Cell Mol Physiol 300:L341–L353. https://doi.org/10.1152/ajplung.00122.2010

6. Sisson TH, Mendez M, Choi K, Subbotina N, Courey A, Cunningham A, Dave A, Engelhardt JF, Liu X, White ES, Thannickal VJ, Moore BB, Christensen PJ, Simon RH (2010) Targeted injury of type II alveolar epithelial cells induces pulmonary fibrosis. Am J Respir Crit Care Med 181:254–263. https://doi.org/10.1164/rccm.200810-1615OC

7. Moore B, Lawson WE, Oury TD, Sisson TH, Raghavendran K, Hogaboam CM (2013) Animal models of fibrotic lung disease. Am J Respir Cell Mol Biol 49:167–79. https://doi.org/10.1165/rcmb.2013-0094TR

8. Della Latta V, Cecchettini A, Del Ry S, Morales MA (2015) Bleomycin in the setting of lung fibrosis induction: from biological mechanisms to counteractions. Pharmacol Res 97:122–130. https://doi.org/10.1016/j.phrs.2015.04.012

9. Mouratis MA, Aidinis V (2011) Modelling pulmonary fibrosis with bleomycin. Curr Opin Pulm Med 17:355–361. https://doi.org/10.1097/MCP.0b013e328349ac2b

10. Mungunsukh O, Griffin AJ, Lee YH, Day RM (2010) Bleomycin induces the extrinsic apoptotic pathway in pulmonary endothelial cells. Am J Physiol Lung Cell Mol Physiol 298:L696–L703. https://doi.org/10.1152/ajplung.00322.2009

11. Cassel SL, Eisenbarth SC, Iyer SS, Sadler JJ, Colegio OR, Tephly LA, Carter AB, Rothman PB, Flavell RA, Sutterwala FS (2008) The Nalp3 inflammasome is essential for the development of silicosis. Proc Natl Acad Sci USA 105:9035–9040. https://doi.org/10.1073/pnas.0803933105

12. Dinis-Oliveira RJ, Duarte JA, Sánchez-Navarro A, Remião F, Bastos ML, Carvalho F (2008) Paraquat poisonings: mechanisms

of lung toxicity, clinical features, and treatment. Crit Rev Toxicol 38:13–71. https://doi.org/10.1080/10408440701669959

13. Martín-Rubí JC, Marruecos-Sant L, Palomar-Martínez M, Martínez-Escobar S (2007) Tratamiento inmunosupresor en las intoxicaciones por paraquat [Immunosuppressive treatment due to paraquat poisoning]. Med Intensiva 31:331–334. https://doi.org/10.1016/s0210-5691(07)74832-5

14. Zheng Q, Liu Z, Shen H, Hu X, Zhao M (2021) Protective effect of toll-interacting protein overexpression against paraquat-induced lung injury in mice and A549 cells through inhibiting oxidative stress, inflammation, and NF-κB signaling pathway. Respir Physiol Neurobiol 286:103600. https://doi.org/10.1016/j.resp.2020.103600

15. Schapochnik A, da Silva MR, Leal MP, Esteves J, Hebeda CB, Sandri S, de Fátima Teixeira da Silva D, Farsky SHP, Marcos RL, Lino-Dos-Santos-Franco A (2018) Vitamin D treatment abrogates the inflammatory response in paraquat-induced lung fibrosis. Toxicol Appl Pharmacol 355:60–67. https://doi.org/10.1016/j.taap.2018.06.020

16. Ahmed MAE, El Morsy EM, Ahmed AAE (2019) Protective effects of febuxostat against paraquat-induced lung toxicity in rats: Impact on RAGE/PI3K/Akt pathway and downstream inflammatory cascades. Life Sci 221:56–64. https://doi.org/10.1016/j.lfs.2019.02.007

17. Guo G, Zhu Y, Wu Z, Ji H, Lu X, Zhou Y, Li Y, Cao X, Lu Y, Talbot P, Liao J, Shi Y, Bu H (2018) Circulating monocytes accelerate acute liver failure by IL-6 secretion in monkey. J Cell Mol Med 22:4056–4067. https://doi.org/10.1111/jcmm

18. Chen H, Cui J, Wang J, Wang Y, Tong F, Tian Y, Gong Y, Ma Y, Liu L, Zhang X (2022) 5-Aminosalicylic acid attenuates paraquat-induced lung fibroblast activation and pulmonary fibrosis of rats. Mol Med Rep 25:58. https://doi.org/10.3892/mmr.2021.12574

19. Hu Y, Qian C, Sun H, Li Q, Wang J, Hua H, Dai Z, Li J, Li T, Ding Y, Yang X, Zhang W (2021) Differences in epithelial-mesenchymal-transition in paraquat-induced pulmonary fibrosis in BALB/C and BALB/C (nu/nu) nude mice. Biomed Pharmacother 143:112153. https://doi.org/10.1016/j.biopha.2021.112153

20. Kovalchuk N, Jilek JL, Van Winkle LS, Cherrington NJ, Ding X (2022) Role of lung P450 oxidoreductase in paraquat-induced collagen deposition in the lung. Antioxidants (Basel) 11:219. https://doi.org/10.3390/antiox11020219

21. SreeHarsha N (2022) Embelin impact on paraquat-induced lung injury through suppressing oxidative stress, inflammatory cascade, and MAPK/NF-κB signaling pathway. J Biochem Mol Toxicol 34:e22456. https://doi.org/10.1002/jbt.22456

22. Pincus SH, Bhaskaran M, Brey RN 3rd, Didier PJ, Doyle-Meyers LA, Roy CJ (2018) Clinical and pathological findings associated with aerosol exposure of macaques to ricin toxin. Toxins (Basel) 7:2121–2133. https://doi.org/10.3390/toxins7062121

23. Chang MW, Chang SS, Lee CC, Sheu BF, Young YR (2008) Hypokalemia and hypothermia are associated with 30-day mortality in patients with acute paraquat poisoning. Am J Med Sci 335:451–456. https://doi.org/10.1097/MAJ.0b013e318157cb6d

24. Ren W, Chen Y, Wang Y, Wang C, Tian M, Gu X, Lv W (2021) Inhibitory effect of pirfenidone on pulmonary fibrosis in patients with acute paraquat poisoning. Am J Transl Res 13:13192–13199

25. Wu J, Song D, Li Z, Guo B, Xiao Y, Liu W, Liang L, Feng C, Gao T, Chen Y, Li Y, Wang Z, Wen J, Yang S, Liu P, Wang L, Wang Y, Peng L, Stacey GN, Hu Z, Feng G, Li W, Huo Y, Jin R, Shyh-Chang N, Zhou Q, Wang L, Hu B, Dai H, Hao J (2020) Immunity-and-matrix-regulatory cells derived from human embryonic stem cells safely and effectively treat mouse lung injury and fibrosis. Cell Res 30:794–809. https://doi.org/10.1038/s41422-020-0354-1

26. Pham T, Rubenfeld GD (2017) Fifty years of research in ARDS. The epidemiology of acute respiratory distress syndrome. A 50th birthday review. Am J Respir Crit Care Med 195:860–870. https://doi.org/10.1164/rccm.201609-1773CP

27. Kelahan LC, Kalaria AD, Filice RW (2017) PathBot: a radiology-pathology correlation dashboard. J Digit Imaging 30:681–686. https://doi.org/10.1007/s10278-017-9969-2

28. Vale JA, Meredith TJ, Buckley BM (1987) Paraquat poisoning: clinical features and immediate general management. Hum Toxicol 6:41–47. https://doi.org/10.1177/096032718700600107

29. Moore BB, Hogaboam CM (2008) Murine models of pulmonary fibrosis. Am J Physiol Lung Cell Mol Physiol 294:L152–L160. https://doi.org/10.1152/ajplung.00313.2007